

Selective and Collective Actuation in Active Solids

P. Baconnier¹, D. Shohat^{1,2}, C. Hernández López^{3,4}, C. Coulais⁵, V. Démery^{1,6}, G. Düring^{3,4}, O. Dauchot^{1,*}

Active solids consist of elastically coupled out-of-equilibrium units performing work^{1–13}. They are central to autonomous processes, such as locomotion, self-oscillations and rectification, in biological systems^{14–25}, designer materials²⁶ and robotics^{27–31}. Yet, the feedback mechanism between elastic and active forces, and the possible emergence of collective behaviours in a mechanically stable elastic solid remains elusive. Here we introduce a minimal realization of an active elastic solid, in which we characterize the emergence of selective and collective actuation resulting from the interplay between activity and elasticity. Polar active agents exert forces on the nodes of a two dimensional elastic lattice. The resulting displacement field nonlinearly reorients the active agents. For large enough coupling, a collective oscillation of the lattice nodes around their equilibrium position emerges. Only a few elastic modes are actuated and, crucially, they are not necessarily the lowest energy ones. Combining experiments with the numerical and theoretical analysis of an agents model, we unveil the bifurcation scenario and the selection mechanism by which the collective actuation takes place. Our findings may provide a new mechanism for oscillatory dynamics in biological systems^{14,19,21,24} and the opportunity for bona-fide autonomy in meta-materials^{32,33}.

Active solids^{1–13} combine the central properties of simple elastic solids and active liquids^{34–39} (Fig.1-a). On one hand the positional degrees of freedom of their constituting units have a well-defined reference state. On the other hand activity endows these units with an additional free degree of freedom in the form of polar, or dipolar, active forces. In active liquids, aligning interactions between these forces lead to collective motion. In active solids these active forces deform the elastic ma-

trix, and induce a strain field, which depends on the forces configuration. This strain tensor will in turn reorient the forces. This generic nonlinear elasto-active feedback, a typical realization of which is the contact inhibition locomotion (CIL) of cells^{14,19}, opens the path towards spontaneous collective excitations of the solid, which we shall call collective actuation. In this work we propose a minimal experimental setting and numerical model, in which we unveil the modal selectivity of collective actuation and its underlying principles.

We consider crystalline lattices with, at the center of each node, an active particle with a fluctuating orientation (Fig.1-b and Methods). Each node has a well defined reference position, but will be displaced by the active particles (Fig.1-c). In contrast, the polarization of each particle is free to rotate and reorients towards its displacement (Fig.1-d, Supplementary Information section 2.2.2 and Movie 1). This nonlinear feedback between deformations and polarizations is characterized by two length-scales: (i) the typical elastic deformation caused by active forces l_e (Fig.1-c) and (ii) the self-alignment length l_a (Fig.1-d). We complement the experiments with numerical simulations of elastically coupled self-aligning active particles⁴⁰ (Methods). In the over-damped, harmonic and noiseless limit, the model reads:

$$\dot{\mathbf{u}}_i = \pi \hat{\mathbf{n}}_i - \mathbb{M}_{ij} \mathbf{u}_j \quad (1a)$$

$$\dot{\hat{\mathbf{n}}}_i = (\hat{\mathbf{n}}_i \times \dot{\mathbf{u}}_i) \times \hat{\mathbf{n}}_i, \quad (1b)$$

where the ratio of the elasto-active and self-alignment lengths, $\pi = l_e/l_a$, which we refer to as the elasto-active feedback, is the unique control parameter. $\hat{\mathbf{n}}_i$'s are the polarization unit vectors, \mathbf{u}_i is the displacement field with respect to the reference configuration and \mathbb{M} is the dynamical matrix (Supplementary Information section 3.1).

If not hold, such an active solid adopts the translational and/or rotational rigid body motion dictated by the presence of zero modes (Movies 2,3), as reported in other theoretical models^{3,5,16}. Here we are interested in stable

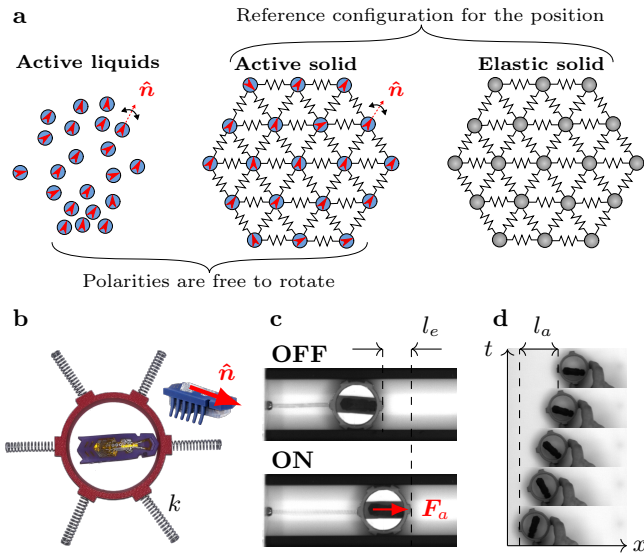


FIG. 1. **Active solids design principle.** **a**, Active solids have positional degrees of freedom with a reference state, and a free to rotate polarity vector in the direction of the active force. **b**, Active unit : a hexbug is trapped in a 3d printed cylinder. **c**, The active component, here confined in a linear track and attached to a spring of stiffness k , produces an active force of amplitude F_0 in the direction of the polarity $\hat{\mathbf{n}}$ and elongates the spring by a length $l_e = F_0/k$. **d**, The mechanical design of the hexbug – mass distribution and shape of the legs – is responsible for its alignment toward its displacement, here imposed manually, of the cylinder (see Supplementary Information for a quantitative measure of the self-alignment length l_a).

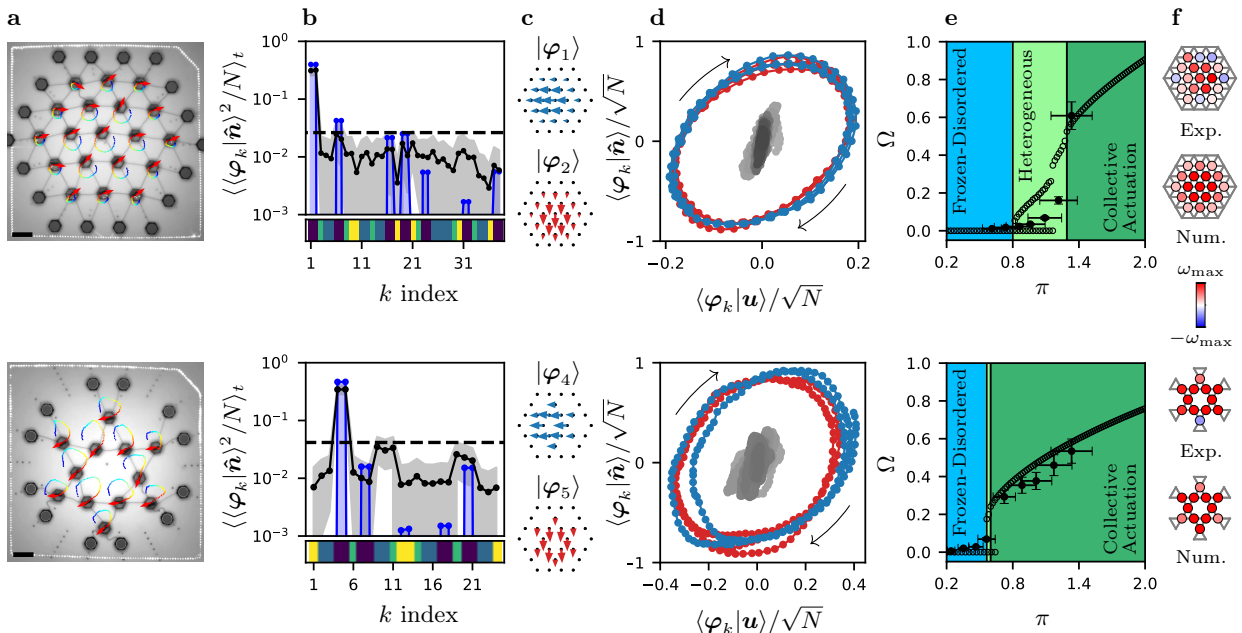


FIG. 2. **Selective and collective actuation in 2d elastic lattices, pinned at their edges** (top) triangular lattice, $N = 19$; (bottom) kagome lattice, $N = 12$: **a**, When embedded in an elastic lattice, a large enough elasto-active feedback π drives the system towards collective actuation dynamics (red arrows: polarities \hat{n}_i ; trajectories color coded from blue to red by increasing time; scale bars: 10 μm). **b**, Spectral decomposition of dynamics on the normal modes of the lattices, sorted by order of growing energies (grey: experiments; blue: numerics). The horizontal dashed lines indicate equipartition. The bottom color bars code for the symmetry class of the modes (Supplementary Information section 7). The gray area represents the $1\text{-}\sigma$ confidence interval on the experimental measurement. **c**, Sketch of the two most excited modes, which are not necessarily the lowest energy ones. **d**, Normal modes components of the active forces as a function of the normal modes components of the displacements (blue/red : projection on **c**, grey : other modes). The symbol size is set to represent to $1\text{-}\sigma$ confidence interval on the experimental measurement. **e**, Transition to the collective actuation regime: average oscillation frequency Ω as a function of π (plain bullets: experiments; open circles: numerics). Background colors code for the dynamical regime (light blue: frozen and disordered; light green: heterogeneous (H); dark green: collective actuation). Triangular: $\pi_{FD} = 0.800$, $\pi_{CA} = 1.29$; kagome: $\pi_{FD} = 0.564$, $\pi_{CA} = 0.600$. The errorbars represent the $1\text{-}\sigma$ confidence intervals, inherited from the uncertainty on the microscopic parameters measurements. **f**, Individual oscillation frequencies ω_i illustrating the coexistence dynamics in experiments and numerical simulations; (triangular lattice: $\pi_{\text{exp}}/\pi_{\text{num}} = 1.22/1.09$; kagome lattice: $\pi_{\text{exp}}/\pi_{\text{num}} = 0.723/0.564$).

elastic solids, with no zero-modes. We therefore explore the emergence of collective dynamics in elastic lattices pinned at their edges. For both the triangular (Fig.2-top) and the kagome (Fig.2-bottom) lattice, we observe a regime where all the lattice nodes spontaneously break chiral symmetry and rotate around their equilibrium position in a collective steady state (Fig.2-a and Movies 5,8). This dynamical and chiral phase, which is reminiscent of oscillations in biological tissues^{15,24}, is clearly different from collective dynamics in active fluids^{35,36} and rigid body motion in active solids^{3,5,9}.

The dynamics are best described when projected on the normal modes of the elastic structure sorted by order of growing energies. The dynamics condensate mostly on two modes (Fig. 2-b), and describe a limit cycle driven by the misalignment of the polarity and the displacements (Fig. 2-d). In the case of the triangular lattice, the selected modes are the two lowest energy ones. Interestingly, in the case of the kagome lattice, these are the fourth and fifth modes, not the lowest energy ones. For both lattices, the selected pair of degenerated modes are strongly polarized along one spatial direction; they are extended and the polarization of the modes in each pair are locally quasi-orthogonal (Fig. 2-c). The numerical simulations confirm the experimental observations

indicating that collective actuation is already present in the harmonic approximation and is not of inertial origin. It also allows for the observation of additional peaks in the spectrum, which belong to the same symmetry class as the two most actuated modes (Fig. 2-b, Supplementary Information section 7). As we shall see below these properties are at the root of the selection principle of the actuated modes.

The transition to the collective actuation regime (Fig. 2-e) is controlled by the elasto-active feedback. The larger it is, the more the particles reorient upon elastic deformations. Below a first threshold π_{FD} , the active solid freezes in a disordered state, with random polarizations and angular diffusion (Movies 4,7). Beyond a second threshold π_{CA} , collective actuation sets in: synchronized oscillations take place and the noiseless dynamics follow a limit cycle, composed of several frequencies in rational ratio (Supplementary Information, section 10.2). In between, the system is heterogeneous (Fig. 2-f and Movie 6), with the oscillating dynamics being favored close to the center, while the frozen disordered regime invades the system layer by layer, from the edges towards the center, as π decreases (Movie 11).

Simulations with increasing values of N , while keeping

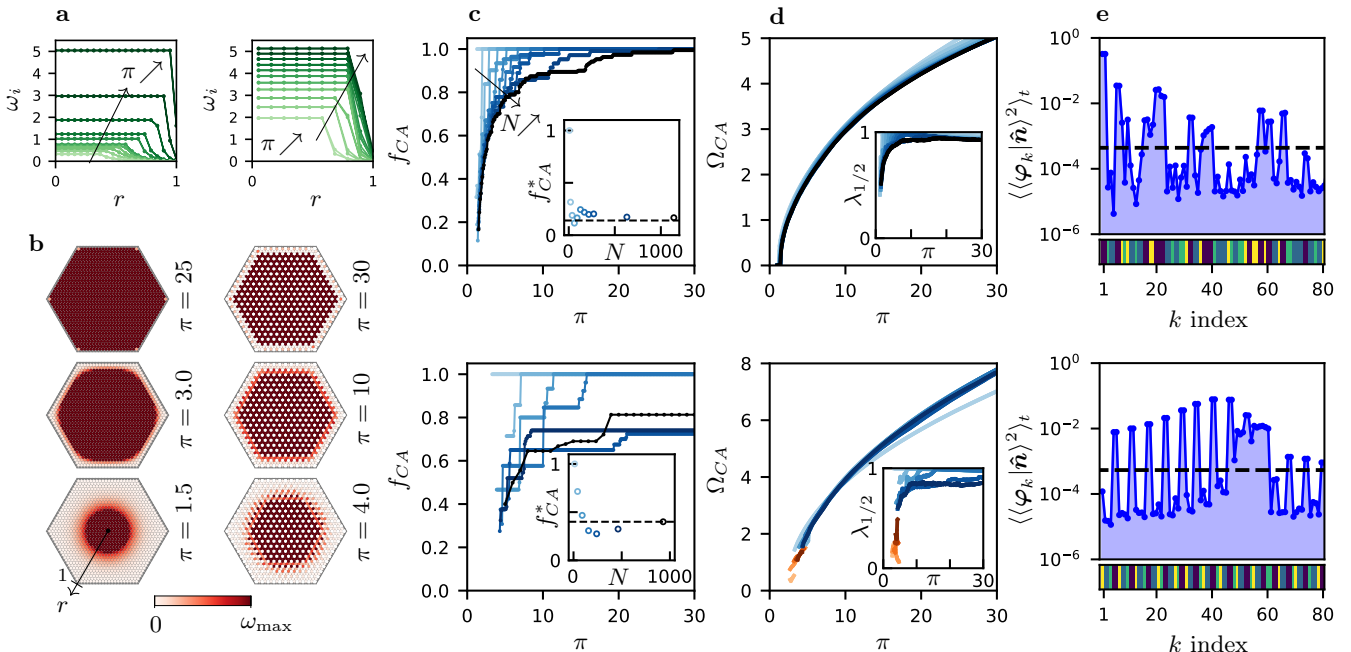


FIG. 3. **Large N lattices.** **a** Radial distribution of the individual oscillation frequencies ω_i (left: triangular lattice, $N = 1141$; right kagome lattice, $N = 930$). Plots are color coded from light to dark green as π increases (triangular lattice: for $\pi \in [1.5, 1.6, 1.7, 1.8, 1.9, 2.0, 2.5, 3.0, 5.0, 10, 30]$; kagome lattice: for $\pi \in [4.0, 5.0, 6.0, 7.0, 8.0, 9.0, 10, 11, 12, 13, 14]$). **b** Spatial distribution of $|\omega_i|$ (left: triangular lattice, $N = 1141$; right kagome lattice, $N = 930$), π values as indicated. **c**, Collective actuation fraction f_{CA} as a function of π for increasing N , color coded from light to dark blue (Inset: f_{CA} at onset of collective actuation saturates to a finite value at large N). **d**, Collective oscillation frequency Ω_{CA} as a function of π for increasing N , same color code (triangular lattices, $N = 7, 19, 37, 61, 91, 127, 169, 217, 271, 631, 1141$; kagome lattice, $N = 12, 42, 90, 156, 240, 462, 930$), (Inset: condensation fraction on the selected symmetry class, $\lambda_{1/2}$ as a function of π for increasing N). **e**, Spectral decomposition of the dynamics on the normal modes of the lattices, sorted by order of growing energies (only the first 80 modes are shown; both for $\pi = 10$). For panels **c,d,e**: top row triangular lattice, bottom row kagome lattice.

the physical size L constant (Methods), indicate that collective actuation subsists for large N (Fig. 3). The successive de-actuation steps converge toward a regular variation of the fraction of nodes activated in the center of the system, f_{CA} (Fig. 3-c-d and Movies 12,13). At the transition to the frozen disordered state, when $\pi = \pi_{FD}$, the fraction of actuated nodes drops discontinuously to zero, from a finite value f_{CA}^* , which decreases with N , but saturates at large N (Fig. 3-d). In the case of the triangular lattices, the collective oscillation frequency, Ω , measured in the region of collective actuation, decreases continuously to zero (Fig. 3-d-top). This is however non generic: in the case of the kagome lattices, very close to the transition, the dynamics condensate on a different set of modes, pointing at the possible multiplicity of periodic solutions. The transition is essentially discontinuous. Most importantly the spectrum demonstrates that, inside the collective actuation regime, the symmetry class of modes that are selected is independent of the system size (Fig. 3-e). The selection of the most actuated modes is again dictated by the geometry of the modes, and not only by their energies. In all cases the condensation level remains large, with a large condensation fraction $\lambda_{1/2}$ (see Methods) for a wide range of values of π (Fig. 3-d-inset).

Altogether our experimental and numerical findings demonstrate the existence of a selective and collective actuation in active solids. This new kind of collective

behaviour specifically takes place because of the elasto-active feedback, that is the reorientation of the active units by the displacement field. The salient features of collective actuation are three-fold: (i) the transition from the disordered phase leads to a chiral phase with spontaneously broken symmetry; (ii) the actuated dynamics are not of inertial origin, take place on a few modes, not always the lowest energy ones, and therefore obey non-trivial selection rules; (iii) the transition follows a coexistence scenario, where the fraction of actuated nodes discontinuously falls to zero. In the remainder of the paper, we unveil the physical origins of these three attributes.

At large scales, the dynamics of the displacement and polarization fields, $\mathbf{U}(\mathbf{r}, t)$ and $\mathbf{m}(\mathbf{r}, t)$, the local averages of, respectively, the microscopic displacements \mathbf{u}_i and the polarizations $\hat{\mathbf{n}}_i$, are obtained from a coarse-graining procedure (see Supplementary Information, section 6) and read:

$$\partial_t \mathbf{U} = \pi \mathbf{m} + \mathbf{F}_e \quad (2a)$$

$$\partial_t \mathbf{m} = (\mathbf{m} \times \partial_t \mathbf{U}) \times \mathbf{m} + \frac{1-m^2}{2} \partial_t \mathbf{U} - D_r \mathbf{m}, \quad (2b)$$

where the elastic force $\mathbf{F}_e[\mathbf{U}]$ is given by the choice of a constitutive relation and the relaxation term $-D_r \mathbf{m}$ results from the noise. Assuming linear elasticity, the frozen phase, in which the local random polarities and displacements average to $\mathbf{U} = \mathbf{0}$ and $\mathbf{m} = \mathbf{0}$, is sta-

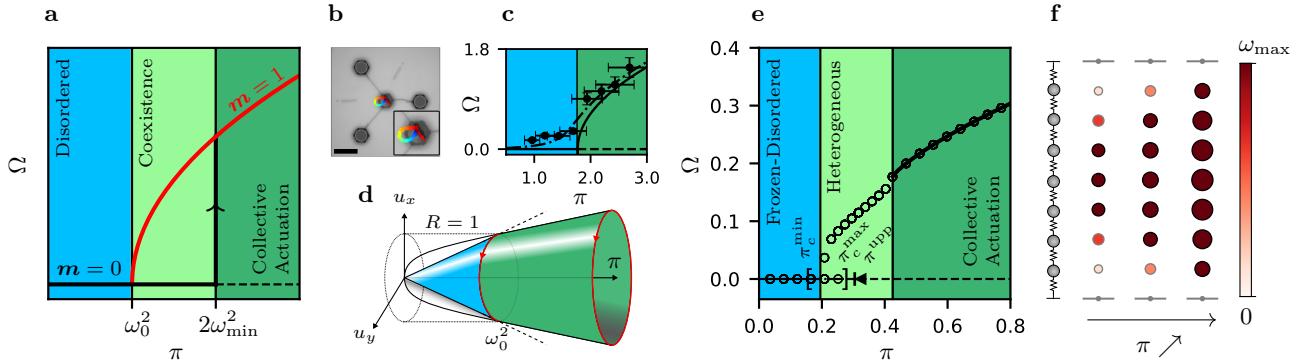


FIG. 4. **Mean field, single particle and 1d lattices phase diagrams.** **a**, At the mean field level, the disordered, $\mathbf{m} = 0$, phase (black line) coexists with the fully polarized, $|\mathbf{m}| = 1$, chiral, $\Omega > 0$, phase (red line) for $\pi \in [\omega_0^2, 2\omega_{\min}^2]$. **b-c-d**, A single active unit connected to the three static vertices of a regular triangle (red arrow: polarity $\hat{\mathbf{n}}$; trajectories color coded from blue to red by increasing time; scale bar: 10 cm; Inset: zoom on the active unit) oscillates with an average rotation frequency Ω increasing with π (**c**); (\bullet): experimental data, (continuous line): analytical expression (Eq. 3), (dot-dashed line): numerical values in the presence of a bias; $\pi_c = 1.77$). The errorbars represent the 1- σ confidence intervals, inherited from the uncertainty on the microscopic parameters measurements. **d**, Phase space structure of the displacements: for $\pi < \omega_0^2$, an infinite set of marginal fixed points forms a circle of radius $R = \pi/\omega_0^2$; for $\pi > \omega_0^2$, all such fixed points are unstable and a limit cycle of radius $R = (\pi/\omega_0^2)^{1/2}$ branches off continuously. **e-f**, The collective actuation in a zero rest length chain of $N = 7$ nodes, pinned at both ends: **e**, average oscillation frequency Ω as a function of π (continuous line: limit cycle found analytically; horizontal lines ($\Omega = 0$): range of existence of only stable (continuous), only unstable (dashed) and coexisting stable and unstable (dot-dashed) fixed points; (\circ): numerical data; same background color as for Fig. 2-e). $\pi_c^{\min} = 0.152$, $\pi_c^{\max} = 0.280$, $\pi_c^{\text{upp}} = 0.304$, $\pi_{FD} = 0.195$, $\pi_{CA} = 0.426$. **f**, Individual oscillation frequencies ω_i for increasing values of $\pi = [0.20, 0.33, 1.0]$, in the $N = 7$ chain. Radii of the colored circles code for the average trajectory radius. Black, respectively gray, contours indicate $R_i \geq 1$ and $R_i \leq 1$.

ble for small elasto-active feedback. It becomes linearly unstable for $\pi > \pi_c^{\text{eg}} = 2\omega_{\min}^2$, where ω_{\min}^2 is the smallest eigenvalue of the linear elastic operator (Supplementary Information, section 6.5). We then look for homogeneous solutions, assuming a condensation on two degenerated and spatially homogeneous modes, such that $\mathbf{F}_e = -\omega_0^2 \mathbf{U}$, with ω_0^2 the eigenfrequency of such modes. For $\pi > \omega_0^2$, we find a polarized chiral phase oscillating at a frequency

$$\Omega = \omega_0 \sqrt{\pi - \omega_0^2}, \quad (3)$$

In the limiting case $D_r = 0$, $|\mathbf{m}| = 1$ (Supplementary Information, section 6.6). The resulting mean field phase diagram (Fig. 4-a) thus captures the existence of the frozen and chiral phases and their phase space coexistence for a finite range of the elasto-active feedback. However, the disordered $\mathbf{m} = \mathbf{0}$, and the polarized chiral oscillating solutions being disconnected, the nature of the transition is controlled by inhomogeneous solutions, which cannot be investigated within perturbative approaches.

Alternatively, we turn ourselves to simpler geometries in which exact results can be obtained. A first important hint at the nature of the transition towards the chiral phase concerns the structure of the phase space, and is best understood from considering the dynamics of a single particle (Fig. 4-b and Movies 9,10 and Supplementary Information section 5). Below $\pi_c = \omega_0^2$, the phase space for the displacements contains an infinite set of marginal fixed points, organized along a circle of radius $R = \pi/\omega_0^2$. At π_c , the escape rate of the polarity, away from its frozen orientation, becomes faster than the restoring dynamics of the displacement. As a result, the later permanently chase the polarity, and the

stable rotation sets in. All fixed points become unstable at once; and a limit cycle of radius $R = (\pi/\omega_0^2)^{1/2}$ and oscillation frequency, $\Omega = \omega_0 \sqrt{\pi - \omega_0^2}$, identical to the one obtained from the mean field approach, branches off continuously (Fig. 4-c-d). Note that the oscillating dynamics does not arise from a Hopf bifurcation, but from the global bifurcation of a continuous set of fixed points into a limit circle.

Understanding how the nonlinear coupling of N such elementary units leads to the selection mechanism of the actuated modes requires a more involved analysis. One sees from Eqs. (1) that any configuration $(\{\hat{\mathbf{n}}_i\}, \{\mathbf{u}_i = \pi \mathbb{M}_{ij}^{-1} \hat{\mathbf{n}}_j\})$ is a fixed point of the dynamics. In contrast with the one particle case, the linear destabilization threshold $\pi_c(\{\hat{\mathbf{n}}_i\})$ depends on the fixed point configuration (Supplementary Information section 4.4). These thresholds are bounded $\pi_c^{\min} \leq \pi_c(\{\hat{\mathbf{n}}_i\}) \leq \pi_c^{\max}$. A first fixed point becomes unstable for $\pi = \pi_c^{\min} = \omega_{\min}^2$, where ω_{\min}^2 is the smallest eigenvalue of the dynamical matrix \mathbb{M} (Supplementary Information section 4.5) and an upper bound for π_c^{\max} (Supplementary Information section 4.6) reads :

$$\pi_c^{\text{upp}} = \min_{\{i,j\}} \left(\frac{\omega_i^2 + \omega_j^2}{c(|\varphi_i\rangle, |\varphi_j\rangle)} \right), \quad (4)$$

The function $c(\bullet, \bullet)$ only depends on the eigenvectors of \mathbb{M} , $\{|\varphi_i\rangle\}$. It is bounded between 0 and 1 and is maximal when the modes $|\varphi_i\rangle$ and $|\varphi_j\rangle$ are extended and locally orthogonal. More specifically, the pair of modes which dominates the dynamics, $\{|\varphi_1\rangle, |\varphi_2\rangle\}$ for the triangular and $\{|\varphi_4\rangle, |\varphi_5\rangle\}$ for the kagome lattice, are precisely the ones that optimize the bound. The construction of this bound is very general. It demonstrates that for

any stable elastic structure, there is a strength of the elasto-active feedback above which the frozen dynamics is unstable and a dynamical regime must set in. It also captures the mode selection in the strongly condensed regime. Our findings about the linear stability of the fixed points for the triangular and kagome lattices are summarized in Extended Data Fig.1.

That some fixed points loose stability does not imply that collective actuation sets in: from these fixed points, the system can either slide to a neighboring stable fixed point or condensate on some dynamical attractor. An exact theory to describe this condensation process is still missing in the general case, but can be formulated in the simpler, yet rich enough, case of a linear chain of N active particles, fixed at both ends. In the zero rest length limit of the springs, the rotational invariance of the dynamical equations ensures that the eigenvalues and eigenvectors of the dynamical matrix are degenerated by pairs of locally orthogonal modes. In such a situation, the limit cycle solution, corresponding to the collective actuation regime, is found analytically (Supplementary Information, section 9.2), leading to a precise transition diagram, illustrated here for $N = 7$ (Fig.4-e). When π exceeds the threshold value π_{CA} , the limit cycle is stable. We have checked that it is the only stable periodic solution, up to $N = 20$. If $\pi_{CA} \leq \pi \leq \pi_c^{\max}$, it coexists with an infinite number of stable fixed points. The evolution of their respective basins of attraction can be largely understood by studying the $N = 2$ case (Supplementary Information section 9.3.1, Fig. S9). For $\pi < \pi_{CA}$, the dynamics leave the limit cycle and become heterogeneous.

The physical origin of the spatial coexistence lies in the normalization constraint of the polarity field, $\|\hat{\mathbf{n}}_i\| = 1$, which translates into a strong constraint over the radii of rotation, namely $R_i \geq 1$ (Supplementary Information, section 9.2.3 and 9.2.4). Whenever R_i becomes unity the polarity and displacement vectors become parallel, freezing the dynamics. The spatial distribution of the R_i is set by that of the modes selected by the collective actuation, with particles closer to the boundaries having typically a smaller radius of rotation than the ones at the center. The threshold value π_{CA} , below which the dynamics leave the limit cycle, is precisely met when the particles at the boundary reach a radius of rotation $R = 1$. For $\pi < \pi_{CA}$, the competition between outer particles, which want to freeze, and the central particles, which want to cycle, leads to the sequential layer by layer de-actuation, illustrated in Fig. 4-f for a linear chain with $N = 7$ and observed experimentally and numerically. The threshold value π_{FD} is reached when, eventually, the remaining particles at the center freeze and the system discontinuously falls into the frozen disordered state.

Altogether we have shown that (i) the chiral phase takes its origin in the one-particle dynamics; (ii) the selection of modes results from the nonlinear elasto-active feedback, which connects the linear destabilization of the fixed points to the spatial extension and local orthogonality of pairs of modes; (iii) the spatial coexistence

emerges from the normalization constraint of the polarity fields.

The role of noise, which was not considered in the numerical and theoretical analysis, is another matter of interest. In the frozen disordered regime, the noise is responsible for the angular diffusion of the polarities amongst the fixed points. In the collective actuation regime the noise level present in the experiment does not alter significantly the dynamics. Numerical simulations confirm that there is a sharp transition at a finite noise amplitude D_c , below which collective actuation is sustained (Extended Data Fig.2-a). For noise amplitude much lower than D_c , the noise merely reduces the mean angular frequency Ω (Extended Data Fig.2-b). Closer to the transition, the noise allows for stochastic inversions of the direction of rotation, restoring the chiral symmetry. (Extended Data Fig.2-c).

Finally, it has been shown very recently, that non symmetrical interactions, together with non conservative dynamics, generically lead to chiral phases⁴¹. Here, the polarity and displacement vectors of a single particle do experience non symmetrical interactions, the phase of the displacement chasing that of the polarity. Mapping the coarse grained equations to the most general equations one can write for rotationally symmetric vectorial order parameters⁴¹, we find that the macroscopic displacement and polarity fields also couple non-symmetrically (Methods). This suggests a possible description of the transition to collective actuation in terms of non reciprocal phase transitions. If this were to be confirmed by a more involved analysis of the large scale dynamics, it would motivate the study of the disordered to chiral phase transition in active solids, which has not been addressed theoretically yet. In the same vein, one may ask whether the coarse-grained system shall obey standard or odd elasticity¹³.

More generally, the recent miniaturization of autonomous active units⁴² opens the path towards the extension of our design principle to the scale of material science. In this context, extending the relation between the structural design of active materials – including the geometry and topology of the lattice, the presence of disorder, the inclusion of doping agents – and their spontaneous actuation offers a wide range of perspectives.

References

1. Koenderink, G. H. *et al.* An active biopolymer network controlled by molecular motors. *Proc. Natl Acad. Sci.* **106**, 15192–15197 (2009).
2. Henkes, S., Fily, Y. & Marchetti, M. C. Active jamming: Self-propelled soft particles at high density. *Phys. Rev. E* **84**, 040301 (2011).
3. Menzel, A. M. & Löwen, H. Traveling and Resting Crystals in Active Systems. *Phys. Rev. Lett.* **110**, 055702 (2013).
4. Berthier, L. & Kurchan, J. Non-equilibrium glass transitions in driven and active matter. *Nat. Phys.* **9**, 310–314 (2013).

5. Ferrante, E., Turgut, A. E., Dorigo, M. & Huepe, C. Elasticity-based mechanism for the collective motion of self-propelled particles with springlike interactions: a model system for natural and artificial swarms. *Phys. Rev. Lett.* **111**, 268302 (2013).
6. Prost, J., Jülicher, F & Joanny, J.-F. Active gel physics. *Nat. Phys.* **11**, 111–117 (Feb. 2015).
7. Ronceray, P., Broedersz, C. P. & Lenz, M. Fiber networks amplify active stress. *Proc. Natl Acad. Sci.* **113**, 2827–2832 (2016).
8. Woodhouse, F. G., Ronellenfitsch, H. & Dunkel, J. Autonomous actuation of zero modes in mechanical networks far from equilibrium. *Phys. Rev. Lett.* **121**, 178001 (2018).
9. Briand, G., Schindler, M. & Dauchot, O. Spontaneously flowing crystal of self-propelled particles. *Phys. Rev. Lett.* **120**, 208001 (2018).
10. Giavazzi, F. *et al.* Flocking transitions in confluent tissues. *Soft Matter* **14**, 3471–3477 (2018).
11. Klongvessa, N., Ginot, F., Ybert, C., Cottin-Bizonne, C. & Leocmach, M. Active glass: Ergodicity breaking dramatically affects response to self-propulsion. *Phys. Rev. Lett.* **123**, 248004 (2019).
12. Maitra, A. & Ramaswamy, S. Oriented active solids. *Phys. Rev. Lett.* **123**, 238001 (2019).
13. Scheibner, C. *et al.* Odd elasticity. *Nat. Phys.* **16**, 475–480 (2020).
14. Abercrombie, M. & Heaysman, J. E. Observations on the social behaviour of cells in tissue culture: II: “Monolayering” of fibroblasts. *Experimental cell research* **6**, 293–306 (1954).
15. Vilfan, A. & Frey, E. Oscillations in molecular motor assemblies. *Journal of physics: Condensed matter* **17**, S3901 (2005).
16. Szabo, B. *et al.* Phase transition in the collective migration of tissue cells: experiment and model. *Phys. Rev. E* **74**, 061908 (2006).
17. Mizuno, D., Tardin, C., Schmidt, C. F. & MacKintosh, F. C. Nonequilibrium mechanics of active cytoskeletal networks. *Science* **315**, 370–373 (2007).
18. Banerjee, S., Utuje, K. J. & Marchetti, M. C. Propagating stress waves during epithelial expansion. *Phys. Rev. Lett.* **114**, 228101 (2015).
19. Smeets, B. *et al.* Emergent structures and dynamics of cell colonies by contact inhibition of locomotion. *Proceedings of the National Academy of Sciences* **113**, 14621–14626 (2016).
20. Bi, D., Yang, X., Marchetti, M. C. & Manning, M. L. Motility-driven glass and jamming transitions in biological tissues. *Phys. Rev. X* **6**, 021011 (2016).
21. Chen, C., Liu, S., Shi, X.-q., Chaté, H. & Wu, Y. Weak synchronization and large-scale collective oscillation in dense bacterial suspensions. *Nature* **542**, 210–214 (2017).
22. Needleman, D. & Dogic, Z. Active matter at the interface between materials science and cell biology. *Nat. Rev. Mater.* **2**, 1–14 (2017).
23. Holmes, D. F. *et al.* Synchronized mechanical oscillations at the cell–matrix interface in the formation of tensile tissue. *Proc. Natl Acad. Sci.* **115**, E9288–E9297 (2018).
24. Peyret, G. *et al.* Sustained oscillations of epithelial cell sheets. *Biophys. J.* **117**, 464–478 (2019).
25. Henkes, S., Kostanjevec, K., Collinson, J. M., Sknepnek, R. & Bertin, E. Dense active matter model of motion patterns in confluent cell monolayers. *Nat. Commun.* **11**, 1–9 (2020).
26. Brandenbourger, M., Locsin, X., Lerner, E. & Coulais, C. Non-reciprocal robotic metamaterials. *Nat. Commun.* **10**, 1–8 (2019).
27. Brambilla, M., Ferrante, E., Birattari, M. & Dorigo, M. Swarm robotics: a review from the swarm engineering perspective. *Swarm Intell.* **7**, 1–41 (2013).
28. Pratisoli, F., Reina, A., Lopes, Y. K., Sabattini, L. & Groß, R. A soft-bodied modular reconfigurable robotic system composed of interconnected Kilobots in MRS (2019), 50–52.
29. Li, S. *et al.* Particle robotics based on statistical mechanics of loosely coupled components. *Nature* **567**, 361–365 (2019).
30. Dorigo, M., Theraulaz, G. & Trianni, V. Reflections on the future of swarm robotics. *Sci. Robot.* **5** (2020).
31. Oliveri, G., van Laake, L. C., Carissimo, C., Miette, C. & Overvelde, J. T. Continuous learning of emergent behavior in robotic matter. *Proc. Natl Acad. Sci.* **118** (2021).
32. Bertoldi, K., Vitelli, V., Christensen, J. & Van Hecke, M. Flexible mechanical metamaterials. *Nature Reviews Materials* **2**, 1–11 (2017).
33. Pishvar, M. & Harne, R. L. Foundations for soft, smart matter by active mechanical metamaterials. *Adv. Sci.* **7**, 2001384 (2020).
34. Toner, J. & Tu, Y. Long-Range Order in a Two-Dimensional Dynamical XY Model: How Birds Fly Together. *Phys. Rev. Lett.* **75**, 4326–4329 (1995).
35. Vicsek, T. & Zafeiris, A. Collective motion. *Physics Reports* **517**, 71–140 (2012).
36. Bricard, A., Caussin, J.-B., Desreumaux, N., Dauchot, O. & Bartolo, D. Emergence of macroscopic directed motion in populations of motile colloids. *Nature* **503**, 95–98 (Oct. 2013).
37. Marchetti, M. C. *et al.* Hydrodynamics of soft active matter. *RMP* **85**, 1143 (2013).
38. Wittkowski, R. *et al.* Scalar φ^4 field theory for active-particle phase separation. *Nat. Commun.* **5**, 1–9 (2014).
39. Peshkov, A., Bertin, E., Ginelli, F. & Chaté, H. Boltzmann-Ginzburg-Landau approach for continuous descriptions of generic Vicsek-like models. *Eur. Phys. J.: Spec. Top.* **223**, 1315–1344 (2014).
40. Dauchot, O. & Démery, V. Dynamics of a self-propelled particle in a harmonic trap. *Phys. Rev. Lett.* **122**, 068002 (2019).
41. Fruchart, M., Hanai, R., Littlewood, P. B. & Vitelli, V. Non-reciprocal phase transitions. *Nature* **592**, 363–369 (2021).
42. Miskin, M. Z. *et al.* Electronically integrated, mass-manufactured, microscopic robots. *Nature* **584**, 557–561 (2020).

Supplementary Information is available in the online version of the paper.

Acknowledgements P.B. was supported by a PhD grant from ED564 “Physique en Ile de France”. D.S. was supported by a Chateaubriand fellowship. G.D. acknowledges support from Fondecyt Grant No. 1210656 and ANID - Millennium Science Initiative Program - Code NCN17_092. We are grateful to Michel Fruchart and Vincenzo Vitelli for fruitful discussions regarding non-reciprocity in elastic materials.

Author Contributions O.D., C.C. and G.D. conceived the project. P.B. and D.S. performed the experiments. P.B., D.S., and O.D. analyzed the experimental results. P.B., V.D., O.D., C.H. and G.D. worked out the theory. All contributed to the writing of the manuscript.

Author Institutions ¹Gulliver UMR CNRS 7083, ESPCI Paris, Université PSL, 75005 Paris, France. ²School of Physics and Astronomy, Tel-Aviv University, Tel Aviv 69978, Israel. ³Instituto de Física, Pontificia Universidad Católica de Chile, Casilla 306, Santiago, Chile. ⁴ANID - Millennium Nucleus of Soft Smart Mechanical Metamaterials, Santiago, Chile. ⁵Van der Waals-Zeeman Institute, Institute of Physics, Universiteit van Amsterdam, Science Park 904, 1098 XH Amsterdam, the Netherlands. ⁶Univ Lyon, ENSL, CNRS, Laboratoire de Physique, F-69342 Lyon, France.